COBEM 2023 27TH INTERNATIONAL CONGRESS OF MECHANICAL ENGENEERING

ABCM Brazilian Society of Mechanical Sciences and Engineering
27th ABCM International Congress of Mechanical Engineering
December 04-08, 2023, Florianópolis-SC, Brazil

COB-2023-1179
NUMERICAL INVESTIGATION OF NON-SMOOTH SOLUTIONS IN FINITE ELASTICITY

Adair Roberto Aguiar
Lucas Almeida Rocha
Department of Structural Engineering, São Carlos School of Engineering, University of São Paulo, Av. Trabalhador Sãocarlense, 400, Cx. P. 359, 13560-590, São Carlos - SP – Brazil
aguiarar@sc.usp.br, lucas.almeida.rocha@usp.br

Abstract. *We consider the problem of an elastic annular disk with uniform thickness in equilibrium in the absence of body force. The disk is fixed on its inner surface and compressed by a uniform pressure on its outer surface. The disk is made of a transversely isotropic material that has a radial axis of symmetry and a constitutive response that is stiffer in the radial direction than in the tangential direction. Material properties of this type are found in carbon fibers with radial microstructure and fiber-reinforced composites. In the context of the classical linear elasticity theory, the solution of this problem predicts large stresses and strains on the inner surface of the disk for a small enough inner radius. The large strains violate the hypothesis of infinitesimal strains upon which the theory is based. A natural constitutive extension of the linear to the nonlinear elasticity theory consists of considering that the disk is made of a transversely isotropic St Venant-Kirchhoff material. In this work, we formulate the disk problem as a minimization problem of the total potential energy functional. We first solve this minimization problem using a standard numerical procedure. We find that there is a critical value of pressure above which the numerical results are not convergent which coincides with the emergence of a jump discontinuity in the deformation gradient. In addition, this critical pressure yields an upper bound for the range of validity of the linear elasticity theory. We then propose a modified numerical procedure that yields convergent results.*

Keywords: *Nonlinear elasticity, Transverse isotropy, Minimization, Non-smooth deformation, Finite element method.*

1. INTRODUCTION

We consider the problem of an elastic annular disk with uniform thickness in equilibrium in the absence of body force. The disk is fixed on its inner surface of radius $R_i > 0$ and compressed by a uniform pressure $p > 0$ on its outer surface of radius $R_e > R_i$. The disk is made of a transversely isotropic material with a radial symmetry axis and a constitutive response that is stiffer in the radial direction than in the tangential direction. Material properties of this type are found in carbon fibers with radial microstructure and fiber-reinforced composites (Christensen, 1994; Daniel and Ishai, 2006).

In the context of the classical linear theory of elasticity, the solution of the disk problem is unique and predicts large stresses and strains on the inner surface of the disk if R_i is small enough (Aguiar *et al.*, 2008). For $R_i = 0$, the stresses go monotonically to minus infinity as we approach the center of the disk for any value of $p > 0$ (Lekhnitskii, 1968). Large strains contradict the basic assumptions upon which the classical linear elasticity theory is founded and should not be taken seriously.

For this reason, it is natural to formulate the disk problem in the context of the nonlinear elasticity theory and to consider an anisotropic St-Venant-Kirchhoff material, for which the strains are assumed to be small, albeit no restrictions are imposed on the displacement gradients. The comparison of the solutions of the disk problem using both the linearly elastic and the anisotropic St Venant-Kirchhoff models allow us to investigate the influence of the nonlinear terms neglected in the linearly elastic model and estimate an upper bound for the value of pressure that can be applied so that the solution of the disk problem in the context of the linear elasticity theory is still valid.

In addition, the anisotropic St-Venant-Kirchhoff model has been used to model the behavior of crystals (Lewandowski and Stupkiewicz, 2018), multilayer composites (Vu-Quoc and Tan, 2003), steel fiber-reinforced concrete (Eik *et al.*, 2015) and the multilayer fiber-reinforced rubber for steel belt and carcass layers in tires (Yamashita *et al.*, 2016). Therefore, the understanding of the behavior predicted by this model in boundary value problems, such as the disk problem, is of great value.

As we will see in the next section, for the class of deformations considered in this work, the anisotropic St Venant-Kirchhoff model corresponds to a non-monotonic relation between radial normal stress and radial stretch. This type of constitutive response may yield non-smooth deformation fields that have a jump discontinuity in its deformation gradient across an interior surface of the disk. In such cases, special numerical strategies are required and certain jump conditions must hold across the surface of discontinuity.

In Section 2, we formulate the disk problem as a problem of minimization of the total potential energy functional. In

addition, we analyze the relation between radial normal stress and radial stretch and the jump conditions that a non-smooth deformation field must satisfy. In Section 3, we use a standard numerical procedure to obtain approximate solutions for the disk problem. We find that there is a value of pressure $\bar{p}$ above which the numerical results do not converge as the mesh is refined, which coincides with the emergence of jump discontinuities in the radial stretch. In Section 4, we present an alternative numerical procedure that yields converging numerical results for $p > \bar{p}$. In Section 5, we present some concluding remarks.

2. THE DISK PROBLEM

2.1 The minimization problem

Let $\mathcal{B} \subset \mathbb{R}^3$ denote the undistorted reference configuration of a homogeneous hyperelastic solid in equilibrium. Points $\mathbf{x} \in \mathcal{B}$ are mapped into points $\mathbf{y} \triangleq \mathbf{f}(\mathbf{x})$, where $\mathbf{f} : \mathcal{B} \to \mathbb{R}^3$ is the deformation field. The boundary $\partial\mathcal{B}$ of $\mathcal{B}$ is composed of two non-intersecting parts, $\partial_1\mathcal{B}$ and $\partial_2\mathcal{B}$, $\partial\mathcal{B} = \partial_1\mathcal{B} \cup \partial_2\mathcal{B}$, $\partial_1\mathcal{B} \cap \partial_2\mathcal{B} = \emptyset$, such that $\mathbf{f} = \bar{\mathbf{f}}$ on $\partial_1\mathcal{B}$, where $\bar{\mathbf{f}}$ is a given function, and the traction field $\bar{\mathbf{t}}$ is applied on $\partial_2\mathcal{B}$. In this work, $\bar{\mathbf{t}}$ is a pressure load given by $\bar{\mathbf{t}} = -p \operatorname{cof} \mathbf{F}\, \mathbf{N}$, where $p > 0$.

We consider the problem of minimization of the total potential energy functional given by (Ciarlet, 1988)

$$\min_{\mathbf{f} \in \mathcal{A}} \mathcal{E}(\mathbf{f}), \qquad \mathcal{E}(\mathbf{f}) = \int_{\mathcal{B}} W(\mathbf{F})\, \mathrm{d}\mathbf{x} + \frac{p}{3} \int_{\partial\mathcal{B}} (\operatorname{cof} \mathbf{F}\, \mathbf{N}) \cdot \mathbf{f}\, \mathrm{d}\mathbf{x}, \tag{1}$$

where $\mathcal{A}$ is the set of kinematically admissible deformation fields, W is the strain energy density function, $\operatorname{cof} \mathbf{F} \triangleq (\det \mathbf{F})\, \mathbf{F}^{-T}$, and $\mathbf{N}$ is the outward unit normal to $\partial\mathcal{B}$.

The minimizer Eq. (1) necessarily satisfies the equilibrium equation

$$\operatorname{Div} \mathbf{P} = \mathbf{0} \quad \text{in } \mathcal{B}, \qquad \mathbf{P} \triangleq \frac{\partial W}{\partial \mathbf{F}}, \tag{2}$$

and the boundary conditions

$$\mathbf{f} = \bar{\mathbf{f}} \quad \text{on } \partial_1\mathcal{B}, \qquad \mathbf{P}\, \mathbf{N} = -p \operatorname{cof} \mathbf{F}\, \mathbf{N} \quad \text{on } \partial_2\mathcal{B}, \tag{3}$$

where $\mathbf{P}$ is the first Piola-Kirchhoff stress tensor. Now, let $\mathcal{S} \subset \mathcal{B}$ divide $\mathcal{B}$ into two non-intersecting sub-regions $\mathcal{B}_+$ and $\mathcal{B}_-$, such that $\mathcal{B} = \mathcal{B}_+ \cup \mathcal{B}_- \cup \mathcal{S}$ and let $\mathcal{A}$ include a deformation field that is continuous, but has a finite jump in its deformation gradient across the internal surface $\mathcal{S}$. Then, Eq. (2.a) holds in $\mathcal{B} \setminus \mathcal{S}$ and a minimizer of Eq. (1) must also satisfy the jump conditions (Abeyaratne, 1983)

$$[\mathbf{P}\, \mathbf{N}]_-^+ = \mathbf{0}, \tag{4}$$

$$[W - \mathbf{F}\, \mathbf{N} \cdot \mathbf{P}\, \mathbf{N}]_-^+ = 0, \tag{5}$$

where $\mathbf{N}$ is a unit outer normal to $\mathcal{S}$ that points to $\mathcal{B}_+$ and $[f]_-^+ \triangleq f^+ - f^-$, with f^+ and f^- denoting the limit values of a field f obtained from approaching a point on $\mathcal{S}$ from $\mathcal{B}_+$ and $\mathcal{B}_-$, respectively. In addition, the continuity of the deformation field on $\mathcal{S}$ implies

$$[\mathbf{F}]_-^+ = \mathbf{a} \otimes \mathbf{N} \qquad \text{on } \mathcal{S}, \tag{6}$$

for some vector field $\mathbf{a} : \mathcal{S} \to \mathbb{R}^3$.

We consider that $\mathcal{B}$ is an annular disk with inner radius $R_i > 0$, outer radius $R_e > R_i$, and unitary thickness. Here, $\partial_1\mathcal{B}$ and $\partial_2\mathcal{B}$ are the inner and outer surfaces of the disk, respectively, $\bar{\mathbf{f}} = \mathbf{x}$, and p is a uniform pressure acting on the outer surface.

The disk is made of a transversely isotropic St Venant-Kirchhoff material with a radial axis of symmetry so that

$$W = \frac{1}{2}\, \mathbf{E} \cdot \mathbb{C}[\mathbf{E}], \qquad \mathbf{E} \triangleq \frac{1}{2}\, (\mathbf{F}^T \mathbf{F} - \mathbf{I}), \tag{7}$$

where $\mathbf{I}$ is the identity tensor and $\mathbb{C}$ is the elasticity tensor, whose components can be written in terms of its nonzero components c_{11}, c_{12}, c_{22}, c_{23}, c_{66} in the usual way; see, for instance, Daniel and Ishai (2006).

Let $\{\mathbf{e}_R, \mathbf{e}_\Theta, \mathbf{e}_Z\}$ denote the usual orthonormal cylindrical basis at $\mathbf{x}$ associated with the cylindrical coordinates (R, Θ, Z), such that $\mathbf{x} = R\, \mathbf{e}_R(\Theta) + Z\, \mathbf{e}_Z$. Similarly, let $\{\mathbf{e}_r, \mathbf{e}_\theta, \mathbf{e}_z\}$ and (r, θ, z) be the corresponding orthonormal cylindrical basis and coordinates, respectively, at $\mathbf{y}$, such that $\mathbf{y} = r\, \mathbf{e}_r(\theta) + z\, \mathbf{e}_z$. Unless stated otherwise, we shall omit the dependence of $\mathbf{e}_R$ and $\mathbf{e}_r$ on Θ and θ, respectively.

We want to find a deformation field $\mathbf{f}$, such that points $\mathbf{x} = (R, \Theta, Z) \in [R_i, R_e] \times [0, 2\pi] \times [0, 1]$ move along radial lines according to

$$\mathbf{f}(R, \Theta, Z) = r(R)\, \mathbf{e}_r(\Theta) + Z\, \mathbf{e}_z\,, \tag{8}$$

which corresponds to a displacement field $\mathbf{u}(\mathbf{x}) \triangleq \mathbf{f}(\mathbf{x}) - \mathbf{x}$ with the form

$$\mathbf{u}(R, \Theta, Z) = u_r(R)\, \mathbf{e}_R\,, \qquad u_r(R) = r(R) - R\,. \tag{9}$$

Since $\mathbf{F} \triangleq \nabla \mathbf{f}$, we have that

$$\mathbf{F} = \nu(R)\, \mathbf{e}_r \otimes \mathbf{e}_R + \tau(R)\, \mathbf{e}_\theta \otimes \mathbf{e}_\Theta + \mathbf{e}_z \otimes \mathbf{e}_Z\,, \qquad \nu(R) \triangleq r'(R)\,, \quad \tau(R) \triangleq r(R)/R\,, \tag{10}$$

where the explicit dependence on $\mathbf{x} = (R, \Theta, Z)$ is omitted and $(\cdot)'$ denotes the derivative with respect to R.

It follows from Eq. (1.b), Eq. (7), Eq. (9.b), and Eq. (10) that the total potential energy functional $\mathcal{E}$ can be written as

$$\begin{aligned}\mathcal{E} = \pi \int_{R_i}^{R_e} \Big(&\frac{c_{11}}{4}\, R\, {u_r'}^4 + c_{11}\, R\, {u_r'}^3 + c_{11}\, R\, {u_r'}^2 + c_{12}\, u_r\, {u_r'}^2 + 2\, c_{12}\, u_r\, u_r' + \frac{c_{12}}{2\, R}\, u_r^2\, {u_r'}^2 + \frac{c_{12}}{R}\, u_r^2\, u_r' \\ &+ \frac{c_{22}}{R}\, u_r^2 + \frac{c_{22}}{R^2}\, u_r^3 + \frac{c_{22}}{4\, R^3}\, u_r^4 \Big)\, \mathrm{d}R + \pi\, p\, \left[(R_e + u_r(R_e))^2 - R_i^2 \right],\end{aligned} \tag{11}$$

where we have used the boundary condition $u_r(R_i) = 0$, since the disk is fixed on its inner surface.

2.2 Remarks on the constitutive response and the jump conditions

We present some remarks on the response of the transversely isotropic St Venant-Kirchhoff material and the jump conditions given by Eq. (4) and Eq. (5) for the disk problem of Section 2.1.

Using Eq. (7.a), Eq. (2.b), and Eq. (10), we can write

$$\mathbf{P} = P_{rr}(R)\, \mathbf{e}_r \otimes \mathbf{e}_R + P_{\theta\theta}(R)\, \mathbf{e}_\theta \otimes \mathbf{e}_\Theta + P_{zz}(R)\, \mathbf{e}_z \otimes \mathbf{e}_Z\,, \tag{12}$$

$$P_{rr}(R) = \hat{P}_{rr}(\tau, \nu) \triangleq \left[c_{11}\, (\nu^2 - 1) + c_{12}\, (\tau^2 - 1) \right] \nu/2, \tag{13}$$

$$P_{\theta\theta}(R) = \hat{P}_{\theta\theta}(\tau, \nu) \triangleq \left[c_{12}\, (\nu^2 - 1) + c_{22}\, (\tau^2 - 1) \right] \tau/2\,, \tag{14}$$

$$P_{zz}(R) = \hat{P}_{zz}(\tau, \nu) \triangleq \left[c_{12}\, (\nu^2 - 1) + c_{23}\, (\tau^2 - 1) \right] /2\,. \tag{15}$$

To obtain the elasticity constants c_{11}, c_{12}, c_{22}, first, we introduce the engineering constants $E_1 = 15$, $E_2 = 1$, $\mathrm{v}_{12} = 0.25, \mathrm{v}_{23} = 0.5$, where E and v denote the Young's modulus and the Poisson ratio, respectively, and the subscripts 1, 2, and 3 denote the radial, tangential, and axial directions, respectively. The values of E_1 and E_2 multiplied by a factor of 10^{10} are, approximately, the constants of a unidirectional carbon/epoxy composite (Daniel and Ishai, 2006). Using the relations $c_{11} = E_1\, (1 - \mathrm{v}_{23})/\bar{\mathrm{v}}$, $c_{12} = E_2\, \mathrm{v}_{12}/\bar{\mathrm{v}}$, and $c_{22} = E_2 \left(1 - \mathrm{v}_{12}^2\, E_2/E_1\right) / \left[\bar{\mathrm{v}}\, (1 + \mathrm{v}_{23})\right]$, where $\bar{\mathrm{v}} \triangleq 1 - \mathrm{v}_{23} - 2\, \mathrm{v}_{12}^2\, E_2/E_1$, we obtain

$$c_{11} = 900/59 \approx 15.2542\,, \qquad c_{12} = 30/59 \approx 0.508475\,, \qquad c_{22} = 239/177 \approx 1.35028\,. \tag{16}$$

In Fig. 1 we show the radial stress $\hat{P}_{rr}$ versus ν for $|\tau| = 0, 1, 2, 4, 6$, where ν and τ are defined in Eq. (10). The importance of this stress component becomes clear later in this section. We see from Fig. 1 that $\hat{P}_{rr}$ is non-monotonic with respect to ν, except in the case $|\tau| = 6$. At the inflection points, we have $\partial \hat{P}_{rr}/\partial \nu = 0$ so that, using Eq. (13), we find that the inflections occur at $\nu = \nu^{\,\mathrm{inf}}$ and $\nu = -\nu^{\,\mathrm{inf}}$, where

$$\nu^{\,\mathrm{inf}} \triangleq \frac{\sqrt{3}}{3} \sqrt{\frac{-\tau^2\, c_{12} + c_{11} + c_{12}}{c_{11}}}\,. \tag{17}$$

In addition, $\hat{P}_{rr}$ is monotonic only if $\nu^{\,\mathrm{inf}} = 0$ or $\nu^{\,\mathrm{inf}} \notin \mathbb{R}$, that is, $|\tau| \geq \bar{\tau}$, where

$$\bar{\tau} \triangleq \sqrt{\frac{c_{11} + c_{12}}{c_{12}}}\,. \tag{18}$$

The above considerations regarding the constitutive response will be used to interpret the numerical results of Section 3 and formulate the modified numerical procedure of Section 4.

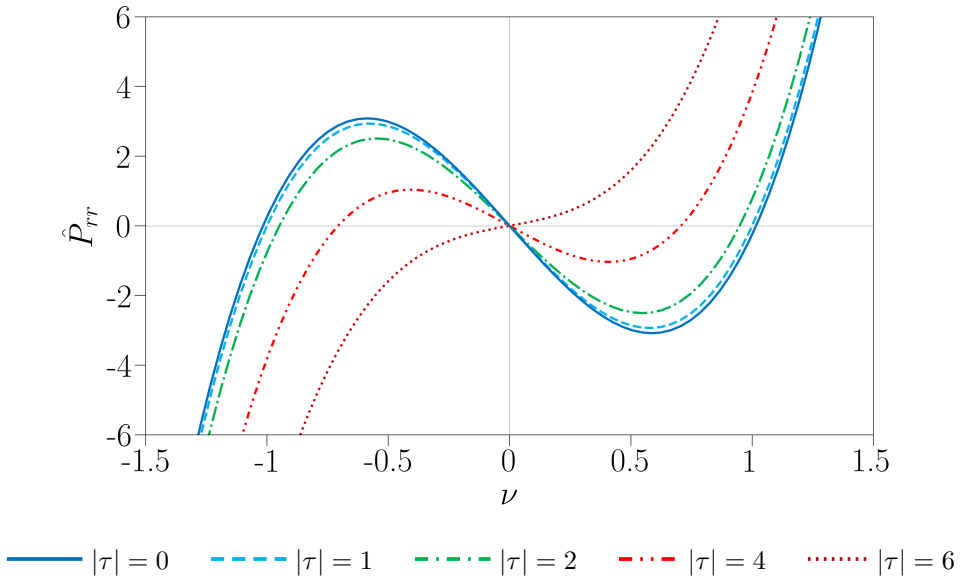

Figure 1. Radial normal stress $\hat{P}_{rr}$ versus ν for different values of τ.

Let us now focus on the jump conditions given by Eq. (4) and Eq. (5). Because of the class of continuous radial deformations given by Eq. (8), τ is continuous and $\mathcal{S}$ is a cylindrical surface with outer unit normal $\mathbf{N} = \mathbf{e}_R$. This together with Eq. (10) implies that the jump condition on $\mathbf{F}$ is given by

$$[\mathbf{F}]^+_- = (\nu^+ - \nu^-)\, \mathbf{e}_r \otimes \mathbf{e}_R \,, \tag{19}$$

which is in agreement with Eq. (6). Then, it follows from Eq. (12) and Eq. (4) with $\mathbf{N} = \mathbf{e}_R$ that P_{rr} is continuous on $\mathcal{S}$. We then have that ν^+ and ν^- must satisfy

$$\hat{P}_{rr}(\nu^+, \tau) = \hat{P}_{rr}(\nu^-, \tau) \triangleq \bar{P}_{rr} \,. \tag{20}$$

If $\nu^+ = \nu^-$, Eq. (20) is trivially satisfied and, from Eq. (19), there is no jump in $\mathbf{F}$, which is not of interest in this work. Thus, in the remainder of this section, we assume $\nu^+ \neq \nu_-$.

Next, we consider the jump condition given by Eq. (5). It follows from Eq. (10), Eq. (12), Eq. (20), and $\hat{W}(\nu, \tau) \triangleq W(\mathbf{F})$ that the jump condition given by Eq. (5) can be written as

$$\hat{W}(\nu^+, \tau) - \hat{W}(\nu^-, \tau) - (\nu^+ - \nu^-)\, \bar{P}_{rr} = 0 \qquad \text{on } \mathcal{S} \,. \tag{21}$$

In view of Eq. (2.b), Eq. (10), Eq. (12), and Eq. (13), we can write $\hat{P}_{rr} = \partial \hat{W} / \partial \nu$ and rewrite Eq. (21) as

$$\int_{\nu_-}^{\nu^+} \hat{P}_{rr}(\nu, \tau)\, \mathrm{d}\nu - (\nu^+ - \nu^-)\, \bar{P}_{rr} = \int_{\nu_-}^{\nu^+} \Big[\hat{P}_{rr}(\nu, \tau) - \bar{P}_{rr} \Big]\, \mathrm{d}\nu = 0 \qquad \text{on } \mathcal{S} \,. \tag{22}$$

For a given τ, Eq. (21) is analogous to Eq. (3.3) of Ericksen (1975). Thus, Eq. (21) holds only if the horizontal line $\hat{P}_{rr}(\cdot, \tau) = \bar{P}_{rr}$ intersects the graph of $\hat{P}_{rr}(\cdot, \tau)$ at three points, such that the two enclosed regions between the graph and the horizontal line have equal areas. This geometric interpretation is more easily seen from Eq. (22) since integrals can be seen as areas under graphs.

Next, observe from Eq. (13) that $\hat{P}_{rr}(\nu, \tau)$ is a cubic polynomial and an odd function of ν, yielding

$$\bar{P}_{rr} = 0 \,, \qquad \nu^+ = -\nu^- \,, \qquad |\nu^+| = |\nu^-| = \sqrt{\frac{-\tau^2\, c_{12} + c_{11} + c_{12}}{c_{11}}} = \sqrt{3}\, \nu^{\,\mathrm{inf}} \,. \tag{23}$$

In addition, since $\det \mathbf{F} = \nu\, \tau$ and τ is continuous on $\mathcal{S}$, $\nu^+ = -\nu^-$ implies that $\det \mathbf{F} \leq 0$ on, at least, one side of $\mathcal{S}$, which is a physically unacceptable behavior. In the next section we will see that there is a value of pressure below which the disk problem has a smooth solution for which this anomalous behavior does not occur.

3. NUMERICAL PROCEDURE AND RESULTS

We consider a Finite Element formulation of the minimization problem given by Eq. (1.a) and Eq. (11), where the displacement field $\mathbf{u}$, which has the form given by Eq. (9), is the unknown variable. Let $\mathcal{V}_h$ be a finite dimensional space

spanned by a set of basis functions $\{\mathbf{w}_i\}$, where h stands for the characteristic length of the finite element. Then, an approximate minimizer $\mathbf{u}_h \in \mathcal{V}_h$ of can be written as

$$\mathbf{u}_h = \sum_{i=1}^{m} s_i \, \mathbf{w}_i \,, \tag{24}$$

where $s_i \in \mathbb{R}$, $i = 1, 2, 3, ..., m$, is a degree of freedom and m is the number of degrees of freedom associated with the discretization. In this work, we use linear finite elements and a Gauss-Legendre quadrature rule with two points.

Let us introduce the vector $\mathbf{s} \triangleq (s_1, s_2, ..., s_m)$ and the function $\mathcal{E}_h(\mathbf{s}) \triangleq \mathcal{E}(\mathbf{x} + \mathbf{u}_h)$. Then, the discrete version of the minimization problem given by Eq. (1.a) and Eq. (11) takes the form

$$\min_{\mathbf{s} \in \mathbb{R}^m} \mathcal{E}_h(\mathbf{s}) \,, \tag{25}$$

where we recall from above that $\mathcal{E}_h(\mathbf{s}) \triangleq \mathcal{E}(\mathbf{x} + \mathbf{u}_h)$ and $\mathcal{E}$ is given by Eq. 11.

To solve the minimization problem given by Eq. (25), we use a standard Newton's method with a unidirectional search; see, for instance, Luenberger and Ye (2008). Thus, starting from an initial guess $\mathbf{s}_0$, we generate a sequence of vectors $\mathbf{s}_k$, $k = 1, 2, 3, ...$, using the recursive formula $\mathbf{s}_{k+1} = \mathbf{s}_k + \alpha_k \, \mathbf{d}_k$, where $\mathbf{d}_k \in \mathbb{R}^m$ is a search direction and $\alpha_k \in \mathbb{R}$ is a step length. We use non-uniform meshes parameterized by $q \in \mathbb{N}$ composed of $N = 24 \times 2^q$ linear finite elements distributed in three intervals: 15×2^q elements in $R_i < R < 0.1\, R_e$, 5×2^q elements in $0.1\, R_e < R < 0.5\, R_e$, and 4×2^q elements in $0.5\, R_e < R < R_e$. This mesh is similar to the meshes used by Aguiar *et al.* (2008) in computational studies of a compressed disk problem. The initial guess used in the numerical procedure corresponds to the undistorted reference configuration, which implies that $\mathbf{s}_0 = \mathbf{0}$. In addition, we consider $R_i = 0.001$ and the material constants given by Eq. (16).

In Fig. 2, we show ν (left) and u_r (right) versus the radius in a neighborhood of the inner surface of the disk for $p = 0.01$. The colored lines correspond to approximate solutions of the nonlinear disk problem using the above numerical procedure with increasing mesh refinements. These lines are almost indistinguishable, which indicates the convergence of the numerical results. The black solid lines correspond to the exact solution of the disk problem in the context of the linear elasticity theory, which is referred to as the linear solution and is given by (Aguiar *et al.*, 2008)

$$\begin{aligned} u_r^{\text{lin}}(R) &= -\frac{R_i}{2\,\kappa}\left[\left(\frac{R}{R_i}\right)^{\kappa} - \left(\frac{R}{R_i}\right)^{-\kappa}\right]\frac{p}{c_{11}\,p_1}\,, \\ p_1 &\triangleq \frac{R_i}{2\,\kappa\,R_e}\left[\left(\kappa - \frac{c_{12}}{c_{11}}\right)\left(\frac{R_i}{R_e}\right)^{\kappa} + \left(\kappa + \frac{c_{12}}{c_{11}}\right)\left(\frac{R_i}{R_e}\right)^{-\kappa}\right], \qquad \kappa \triangleq \sqrt{\frac{c_{22}}{c_{11}}}\,. \end{aligned} \tag{26}$$

We see from Fig. 2 that the radial stretch ν of the nonlinear solution is very similar to that of the linear solution, except in a small neighborhood of $R = R_i$, where it deviates from its linear counterpart by up to 5.8%. In addition, compared to the linear solution, the nonlinear solution predicts a disk with a less stiff response for the displacement, as can be observed from u_r shown in Fig. 2. We have verified that, in comparison with u_r^{lin}, which is given by Eq. (26), u_r of the nonlinear solution has a greater absolute value in the whole disk and is 1.0% larger at $R = R_e$.

In Fig. 3, we show numerical results concerning $p = 0.05$. We show ν (left) and P_{rr} (right) versus the radius in a neighborhood of $R = R_i$. These results were obtained using the mesh parameterized by $q = 8$. We see from this figure that, near $R = 0.003$, ν is not continuous; instead, it has multiple jump discontinuities. These jumps are associated with the non-monotonicity of P_{rr} with respect to ν. As we have seen in the discussion of Fig. 1, given $|\tau| < \bar{\tau}$, there is an interval of P_{rr} where P_{rr} can be associated with three distinct values of ν. In fact, observe from Fig. 3 that P_{rr} is continuous, even though ν is not. The jump discontinuities in ν do not satisfy Eq. (23); therefore, they do not correspond to a minimizer of the considered minimization problem given by Eq. (1.a) and Eq. (11). In addition, we have verified that, for $p = 0.05$, the numerical results do not converge. Different meshes yield numerical approximations of ν with jump discontinuities that do not converge to a limit function.

The above discussion has two outcomes. First, we need a different numerical procedure to find a minimizer of the minimization problem. This will be done in the next section. Second, there is a value of $p = \bar{p} \in (0.01, 0.05)$ below which the nonlinear disk problem has a smooth solution close to the linear solution. For $p > \bar{p}$, the nonlinear solution is not smooth and cannot be found using the above numerical procedure. In the remainder of this section, we focus on $\bar{p}$.

Using the meshes corresponding to $q = 6, 8, 10, 12$, we have found $\bar{p} = 0.018, 0.01400, 0.01383, 0.01379$, respectively, which seems to converge to a limit value as the mesh is refined. We have seen from the discussion of Eq. (23) that a non-smooth minimizer of the minimization problem given by Eq. (1.a) and Eq. (11) corresponds to a solution that predicts a region where the determinant of the deformation gradient is negative, which is not physically acceptable. Therefore, $\bar{p} = 0.01379$ can be viewed as an upper bound for p, so that the considered nonlinear model yields physically plausible results.

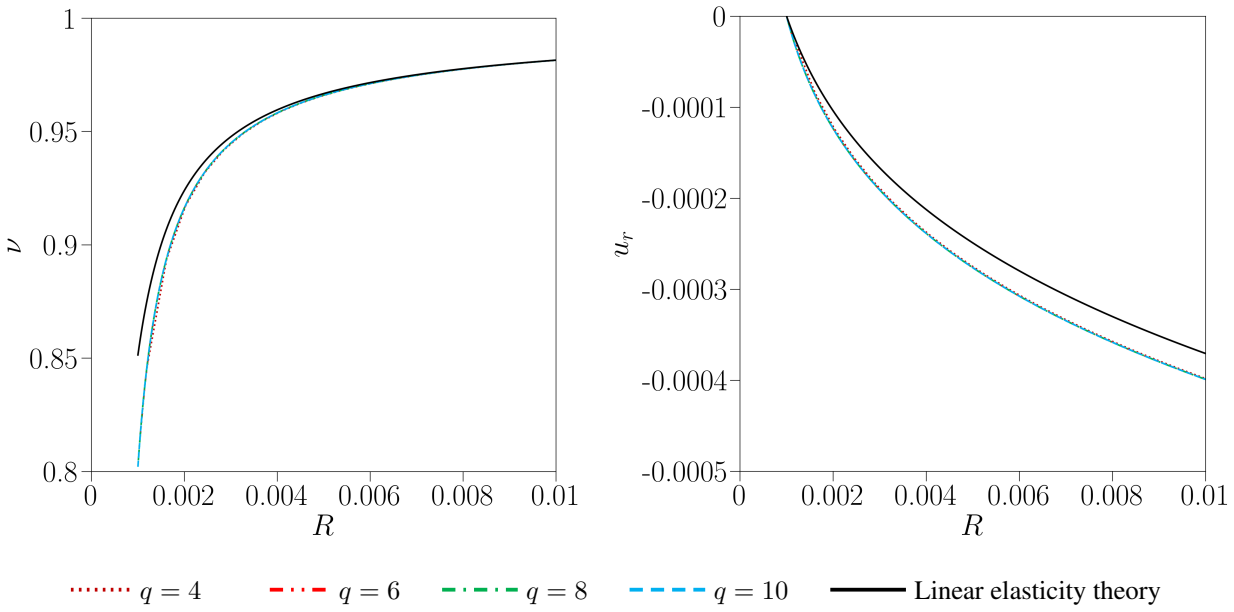

Figure 2. Radial stretch ν and radial displacement u_r versus R for $p = 0.01$.

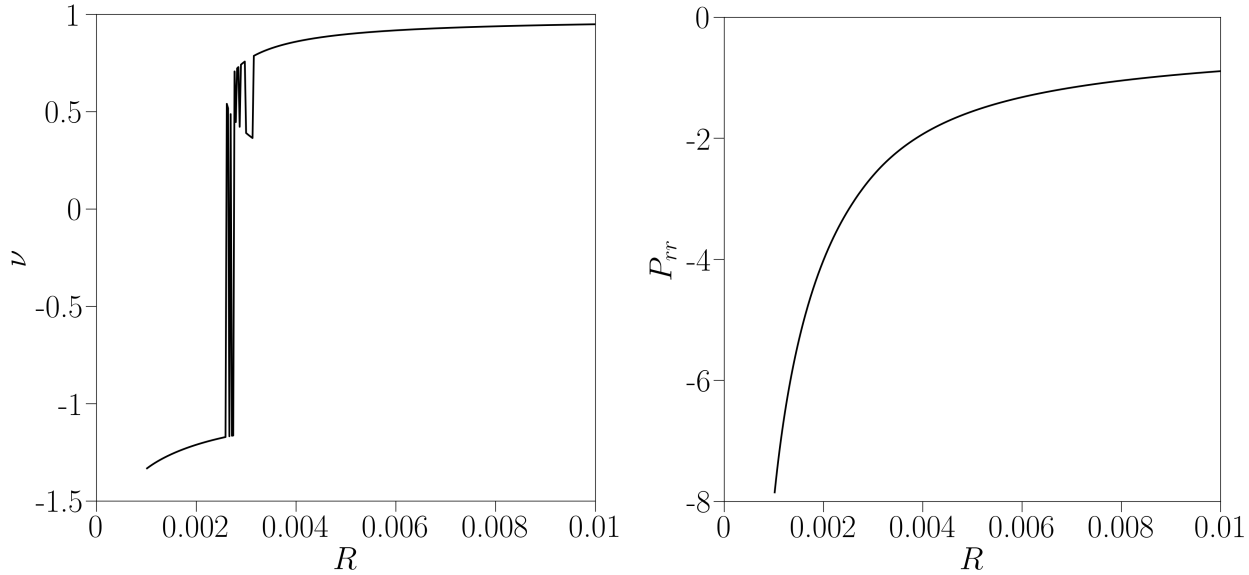

Figure 3. Radial stretch ν and radial normal stress P_{rr} versus R for $p = 0.05$ obtained with $q = 8$.

In the context of the classical linear elasticity theory, there is a critical value of pressure that yields $\det \mathbf{F} = 0$, which is given by $\bar{p}^{\,\mathrm{lin}} = c_{11}\, p_1 \approx 0.06710$, where p_1 is given by Eq. (26) (Aguiar *et al.*, 2008). Since $\bar{p}^{\,\mathrm{lin}} > \bar{p}$, $\bar{p}$ is an upper bound for the pressure below which the linear theory is valid.

4. MODIFIED NUMERICAL PROCEDURE AND RESULTS

We have seen in the previous section that the numerical procedure defined therein fails to yield convergent numerical results when $p > \bar{p}$ because of the non-monotonic relation between P_{rr} and ν and the emergence of jump discontinuities in ν. Here, we propose a modified numerical procedure to solve this issue. The idea is to use a penalty formulation to restrict the jump in ν to occur at a position $R = R_{\mathcal{S}}$ and then search for the value of $R_{\mathcal{S}}$ that minimizes the total potential energy functional. For that, we introduce the penalty functional

$$\mathcal{P}(\mathbf{u}, R_{\mathcal{S}}) \triangleq \delta \left[\int_{\mathcal{B}_-} \max\left(0, \nu^{\inf} + \nu\right)^2 \mathrm{d}\mathbf{x} + \int_{\mathcal{B}_+} \max\left(0, \nu^{\inf} - \nu\right)^2 \mathrm{d}\mathbf{x} \right] \geq 0\,, \tag{27}$$

where $\nu^{\inf}$ is given by Eq. (17), $\delta > 0$ is a penalty parameter, $\mathcal{B}_- = \{\mathbf{x} \in \mathcal{B} \,|\, R_i < R < R_{\mathcal{S}}\}$, and $\mathcal{B}_+ = \{\mathbf{x} \in \mathcal{B} \,|\, R_{\mathcal{S}} < R < R_e\}$. We see from the above equation that $\mathcal{P}$ is null if and only if $\nu \geq \nu^{\inf}$ in $\mathcal{B}_+$ and $\nu \leq -\nu^{\inf}$ in $\mathcal{B}_-$. In addition, $R_{\mathcal{S}}$ is not limited to be in the interval $[R_i, R_e]$; for instance, $R_{\mathcal{S}} < R_i$ means that $\mathcal{B}_- = \emptyset$ and $\mathcal{B}_+ = \mathcal{B}$.

We consider the bi-level minimization problem

$$\min_{R_{\mathcal{S}} \in \mathbb{R}} \; \min_{\mathbf{s} \in \mathbb{R}^m} \mathcal{F}(\mathbf{s}, R_{\mathcal{S}}) \,, \qquad \mathcal{F}(\mathbf{s}, R_{\mathcal{S}}) = \mathcal{E}_h(\mathbf{s}) + \mathcal{P}_h(\mathbf{s}, R_{\mathcal{S}}) \,, \tag{28}$$

where we have used Eq. (24) to define $\mathcal{P}_h(\mathbf{s}, R_{\mathcal{S}}) \triangleq \mathcal{P}(\mathbf{u}_h, R_{\mathcal{S}})$. The lower-level problem is a minimization problem in the vector variable $\mathbf{s}$ parameterized by $R_{\mathcal{S}}$. The upper-level problem is a minimization problem in the scalar variable $R_{\mathcal{S}}$, which we solve by using the golden-section search. See, for instance, Luenberger and Ye (2008).

We set the initial search interval of the golden-section search to be $[0.9\, R_i, 0.01\, R_e]$. At each iteration of this method, we solve the lower-level minimization problem for a given $R_{\mathcal{S}}$ using the standard numerical procedure presented in the previous section. As we increase the value of the penalty parameter δ, the solution of this lower-level minimization problem is expected to converge to a deformation field such that $\mathcal{P}_h(\mathbf{s}) = 0$. Then, we evaluate the corresponding $\mathcal{F}(\mathbf{s}, R_{\mathcal{S}})$ and proceed to the next iteration, where the search interval is reduced. We repeat these iterations until the search interval is smaller than a certain tolerance.

We now reconsider the case $p = 0.05$ using the above modified numerical procedure with $\delta = 1000$ in Eq. (27). Recall from the discussion of Fig. 3 that, for this value of pressure, the standard numerical procedure of the previous section has failed to yield convergent numerical results. In Fig. 4 we show ν (left) and P_{rr} (right) versus the radius in a neighborhood of the inner surface of the disk. The colored lines refer to approximate solutions of the nonlinear disk problem obtained with a sequence of increasing mesh refinements. The black solid lines refer to the corresponding fields, either ν or P_{rr}, obtained with the linear solution, which is given by Eq. (26). We see from this figure that the numerical approximations of both ν and P_{rr} seem to converge to limit functions that satisfy Eq. (23) and are considerably different from their linear counterparts near the inner surface of the disk. We have verified that, for the most refined mesh, which corresponds to $q = 10$, the jump discontinuity of ν occurs at the position $R_{\mathcal{S}} = 0.00554$ where $\nu^- \approx -1.0093$, $\nu^+ \approx 1.0094$, and $\bar{P}_{rr} \approx -0.0016$.

Recall from above that our main interest here is to validate the modified numerical procedure presented in this section, rather than interpreting the physical meaning of the nonlinear and linear solutions. Recall from the previous section that, for $p > \bar{p} \approx 0.01379$, the nonlinear solution predicts material overlapping in a region inside the disk and the strains are too large to be considered in the range of validity of the classical linear elasticity theory. The numerical procedure can be employed in the investigation of phase transition problems for which analogous curves of Fig. 1 are used; a notable example of which is the Ericksen's bar problem (Ericksen, 1975).

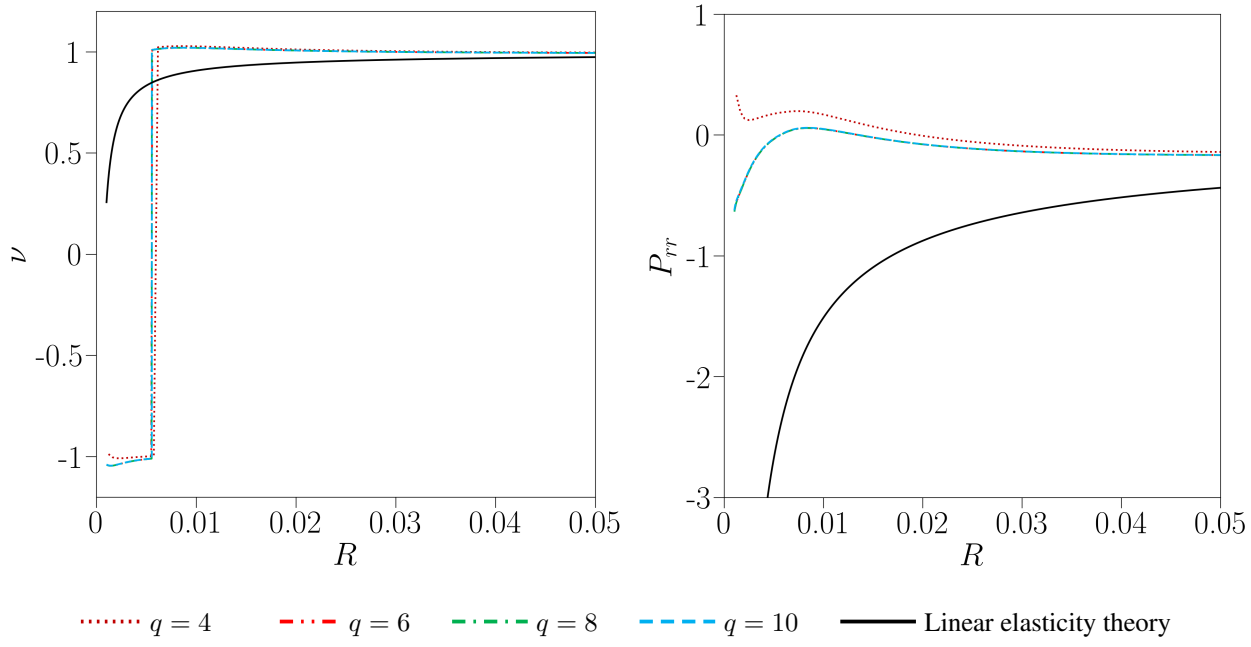

Figure 4. Radial stretch ν and radial normal stress P_{rr} versus R for $p = 0.05$.

5. CONCLUSIONS

We have considered the problem of an elastic annular disk in equilibrium in the absence of body force. The disk is fixed on its inner surface and compressed by a uniform pressure $p > 0$ on its outer surface. The disk is made of a transversely isotropic material with a radial symmetry axis and a nonlinear constitutive response that is stiffer in the radial direction than in the tangential direction. We have formulated the disk problem as a minimization problem of the total potential energy functional. Using a standard numerical procedure, we have found that there is a pressure $\bar{p}$ below which the solution of this nonlinear disk problem is similar to the solution of the disk problem in the context of the linear elasticity theory. For $p > \bar{p}$, the solution of the nonlinear disk problem is not smooth, and requires an alternative numerical procedure to be found. In addition, $\bar{p}$ serves as an upper bound for the pressure below which the solution of the linear disk problem falls in the range of validity of the classical linear elasticity theory.

6. ACKNOWLEDGEMENTS

The authors acknowledge the support of the National Council for Scientific and Technological Development (CNPq), grant n° 306832/2022-4, São Paulo Research Foundation (FAPESP), grant n° 2022/07083-8, and Coordination for the Improvement of Higher Education Personnel (CAPES) – Finance Code 001.

7. REFERENCES

Abeyaratne, R.C., 1983. "An admissibility condition for equilibrium shocks in finite elasticity". *Journal of Elasticity*, Vol. 13, No. 2, pp. 175–184. ISSN 0374-3535. doi:10.1007/BF00041234.

Aguiar, A.R., Fosdick, R.L. and Sanchez, J., 2008. "A study of penalty formulations used in the numerical approximation of a radially symmetric elasticity problem". *Journal of Mechanics of Materials and Structures*, Vol. 3, No. 8. doi: 10.2140/jomms.2008.3.1403.

Christensen, R.M., 1994. "Properties of carbon fibers". *Journal of the Mechanics and Physics of Solids*, Vol. 42, No. 4, pp. 681–695. doi:10.1016/0022-5096(94)90058-2.

Ciarlet, P.G., 1988. *Mathematical elasticity, volume I: Three-dimensional elasticity*. North-Holand, Amsterdam. ISBN 0444702598.

Daniel, I.M. and Ishai, O., 2006. *Engineering Mechanics of Composite Materials*. Number v. 13 in Engineering mechanics of composite materials. Oxford University Press, New York, 2nd edition. ISBN 9780195150971.

Eik, M., Puttonen, J. and Herrmann, H., 2015. "An orthotropic material model for steel fibre reinforced concrete based on the orientation distribution of fibres". *Composite Structures*, Vol. 121, pp. 324–336. ISSN 02638223. doi: 10.1016/j.compstruct.2014.11.018.

Ericksen, J.L., 1975. "Equilibrium of bars". *Journal of Elasticity*, Vol. 5, No. 3-4, pp. 191–201. ISSN 0374-3535. doi:10.1007/BF00126984.

Lekhnitskii, S.G., 1968. *Anisotropic plates*. Gordon & Breach, New York. ISBN 9782881242007.

Lewandowski, M.J. and Stupkiewicz, S., 2018. "Size effects in wedge indentation predicted by a gradient-enhanced crystal-plasticity model". *International Journal of Plasticity*, Vol. 109, pp. 54–78. ISSN 07496419. doi: 10.1016/j.ijplas.2018.05.008.

Luenberger, D.G. and Ye, Y., 2008. *Linear and Nonlinear Programming*, Vol. 116 of *International Series in Operations Research & Management Science*. Springer US, New York, NY. ISBN 978-0-387-74502-2. doi:10.1007/978-0-387-74503-9.

Vu-Quoc, L. and Tan, X., 2003. "Optimal solid shells for non-linear analyses of multilayer composites. I. Statics". *Computer Methods in Applied Mechanics and Engineering*, Vol. 192, No. 9-10, pp. 975–1016. ISSN 00457825. doi:10.1016/S0045-7825(02)00435-8.

Yamashita, H., Jayakumar, P. and Sugiyama, H., 2016. "Physics-Based Flexible Tire Model Integrated With LuGre Tire Friction for Transient Braking and Cornering Analysis". *Journal of Computational and Nonlinear Dynamics*, Vol. 11, No. 3. ISSN 1555-1415. doi:10.1115/1.4032855.

8. RESPONSIBILITY NOTICE

The authors are solely responsible for the printed material included in this paper.